



1 **Estimation of oceanic sub-surface mixing under a severe cyclonic storm**
2 **using a coupled atmosphere-ocean-wave model**

3 Kumar Ravi Prakash, Tanuja Nigam, Vimlesh Pant

4 Centre for Atmospheric Sciences, Indian Institute of Technology Delhi, New Delhi-110016

6 **Abstract**

7 A coupled atmosphere-ocean-wave model used to examine mixing in the upper oceanic
8 layers under the influence of a very severe cyclonic storm Phailin over the Bay of Bengal (BoB)
9 during 10-14 October 2013. Model simulations highlight prominent role of cyclone induced near-
10 inertial oscillations in sub-surface mixing up to the thermocline depth. The inertial mixing
11 introduced by the cyclone played central role in deepening of thermocline and mixed layer depth
12 by 40 m and 15 m, respectively. A detailed analysis of inertial oscillation kinetic energy generation,
13 propagation, and dissipation was carried out at a location in northwestern BoB. The peak
14 magnitude of kinetic energy in baroclinic and barotropic currents found to be $1.2 \text{ m}^2 \text{ s}^{-2}$ and 0.3×10^{-2}
15 $\text{m}^2 \text{ s}^{-2}$, respectively. The power spectrum analysis suggested a dominant frequency operative in
16 sub-surface mixing was associated with near-inertial oscillations. The peak strength of $0.84 \text{ m}^2 \text{ s}^{-1}$
17 1 in zonal baroclinic current found at 14 m depth. The baroclinic kinetic energy remain higher ($>$
18 $0.03 \text{ m}^2 \text{ s}^{-2}$) during 11-12 October and decreased rapidly thereafter. The wave-number rotary
19 spectra identified the downward propagation, from surface up to the thermocline, of energy
20 generated by inertial oscillations. A quantitative analysis of shear generated by the near-inertial
21 baroclinic current showed higher shear generation at 40-80 m depth during peak surface winds.
22 Analysis highlights that greater mixing within the mixed layer take place where the eddy kinetic
23 diffusivity was high ($> 6 \times 10^{-11} \text{ m}^2 \text{ s}^{-1}$). The turbulent kinetic energy dissipation rate increased from
24 4×10^{-14} to $2.5 \times 10^{-13} \text{ W kg}^{-1}$ on approaching the thermocline that dampened mixing process further
25 downward into the thermocline layer.

26

27 **1. Introduction**

28 The Bay of Bengal (BoB), a semi-enclosed basin in the northeastern Indian Ocean, consists
29 of surplus near-surface fresh water due to large precipitation and runoff from the major river



30 systems of Indian subcontinent (Varkey et al., 1996; Rao and Sivakumar, 2003; Pant et al., 2015).
31 Presence of fresh water leads to salt-stratified upper ocean water column and formation of barrier
32 layer (BL), a layer sandwiched between bottom of the mixed layer (ML) and top of the
33 thermocline, in the BoB (Lukas and Lindstrom, 1991; Vinayachandran et al., 2002; Thadathil et
34 al., 2007). The BL restricts entrainment of colder waters from thermocline region into the mixed
35 layer thereby, maintains warmer ML and sea surface temperature (SST). The warmer SST together
36 with higher tropical cyclone heat potential (TCHP) makes the BoB as one of the active regions for
37 cyclogenesis (Suzana et al. 2007; Yanase et al. 2012, Vissa et al. 2013). Majority of tropical
38 cyclones generate during the pre-monsoon (April-May) and post-monsoon (October-November)
39 seasons (Alam et al., 2003; Longshore, 2008). The number of cyclones and their intensity is highly
40 variable in seasonal and interannual time scales. The stratification of the Ocean is one of the
41 important factor to drive the ocean response of the tropical cyclone. The BL formation in the BoB
42 is associated with the strong stratification due to the peak discharge from rivers in the post-
43 monsoon season. The intensity of the cyclone largely depend on the degree of stratification (Neetu
44 et al. 2012; Li et al. 2013).

45 Mixing in the water column has an important role in energy and material transference.
46 Mixing in the ocean can be introduced by the different agents such as wind, current, tide, eddy,
47 and cyclone. Mixing due to tropical cyclones is mostly limited to the upper ocean but the cyclone
48 induced internal waves can affect the subsurface mixing. Several studies have observed that the
49 mixing in the upper oceanic layer is introduced due to generation of near inertial oscillations (NIO)
50 during the passage of tropical cyclones (Gonella, 1971; Shay et al., 1989; Johanston et al., 2016).
51 This mixing is responsible for deepening of ML and shoaling of thermocline (Gill, 1984). The
52 vertical mixing caused by storm induced NIO has significant impact on the upper ocean variability
53 (Price, 1981). The NIO are also found to be responsible for the decrement of SST along the cyclone
54 track (Chang and Anthes, 1979; Leipper, 1967; Shay et al., 1992; Shay et al., 2000). This decrease
55 in SST is caused by the entrainment of cool subsurface thermocline water in the mixed layer into
56 the immediate overlying layer of water. This cooling of surface water is one of the component of
57 the decaying mechanism of the stormy event (Cione and Uhlhorn, 2003). There is a remarkable
58 difference in the magnitude of this cooling of surface temperature moving on the highly stratified
59 to less or weakly stratified bay locations those are falling at the rightward to the cyclone track
60 (Jacob, 2003; Price et al., 1981).



61 The near inertial process can be analyzed from the baroclinic component of currents. The
62 vertical shear of horizontal baroclinic velocities that is interrelated to buoyancy oscillations of
63 surface layers are utilized in various studies to have an adequate understanding of the mixing
64 associated with high frequency oscillations i.e. NIO (Zhang et al., 2014). The shear generated due
65 to NIO is one of the important factor other than the wind stress for the intrusion of the cold
66 thermocline water into the ML during near inertial scale mixing (Price et al., 1978; Shearman,
67 2005; Burchard and Rippeth, 2009). The alternative upwelling and downwelling features of the
68 temperature profile are an indication of the inertial mixing. The Kinetic energy bounded with these
69 components of current shows a rise in magnitude at right side of cyclone track (Price et al., 1981;
70 Sanford et al., 1987; Jacob, 2003). The reason for this high magnitude of kinetic energy is linked
71 with strong wind and rotating wind vector condition of the storm.

72 In several studies (Chang et al., 2008; Lin et al., 2008; Shang et al., 2008; Lin et al., 2003;
73 Zhao et al., 2009), upper Ocean response for various cyclonic events is also inspected and proved
74 for the enhancement of primary productivity during post cyclone state of the Ocean. At the time
75 when storm is active and prior to it, the surface concentration of chlorophyll-a (Chl-a), a proxy for
76 the concentration of primary productivity is comparatively lower than that of the post-cyclonic
77 state of ocean surface (Sarangi, 2011, Latha et al., 2015). This increment in the chlorophyll is
78 dependent on the relative entrainment of the cool subsurface water, enriched in nutrient under the
79 influence of energetic near inertial wave mixing caused by the tropical cyclones.

80 Aim of this paper is to understand and quantify the near inertial mixing due to the Phailin,
81 a very severe cyclonic storm (VSCS) in the BoB. The study also focus on analyzing the subsurface
82 distribution of NIO with its vertical mixing potential. Further, the study quantifies the shear
83 generated mixing and the kinetic energy of these baroclinic mode of horizontal current varying in
84 the vertical section at a selected location during the active period of cyclone. The dissipation rate
85 of NIO and turbulent eddy diffusivity are quantified.

86 **2. Data and Methodology**

87 **2.1 Model details**

88 Numerical simulations during the period of VSCS Phailin were carried out using the
89 coupled Ocean-Atmosphere-wave-Sediment transport (COAWST), described in detail by Warner



90 et al. (2010). COAWST modeling system couples the three-dimensional oceanic model Regional
91 Ocean Modeling System (ROMS), the atmospheric model Weather Research and Forecasting
92 (WRF), and the wind wave generation and propagation model Simulating Waves Nearshore
93 (SWAN). ROMS model used for the study is a free surface, primitive equation, sigma coordinate
94 model. ROMS is a hydrostatic ocean model that solves finite difference approximations of the
95 Reynolds averaged Navier-stokes equations (chassignet et al 2000; Haidvogel et al. 2000,
96 Haidvogel et al. 2008; Shchepetkin and McWilliams 2005). The atmospheric model component in
97 the COAWST is a non-hydrostatic, compressible model Advanced Research Weather Research
98 Forecast Model (WRF-ARW), described in Skamarock et al., (2005). It has different schemes for
99 representation of boundary layer physics and physical parameterizations of sub-grid scale
100 processes. In the COAWST modeling system, appropriate modifications were made in the code of
101 atmospheric model component to provide an improved bottom roughness from the calculation of
102 the bottom stress over the ocean (Warner et al., 2010). Further, the momentum equation is modified
103 to improve the representation of surface waves. The modified equation needs the additional
104 information of wave energy dissipation, propagation direction, wave height, wave length that are
105 obtained from wave component of the COAWST model.

106 The spectral wave model SWAN is designed for shallow water. The wave action balance
107 equation is solved in the wave model for both spatial and spectral spaces (Booij et al. 1999). In the
108 COAWST, the ocean model ROMS simulated free surface elevations (ELV), and current (CUR)
109 are provided to the wave model SWAN. The Kirby and Chen (1998) formulation has been used
110 for the computation of current. The Model Coupling Toolkit (MCT) used as a coupler in the
111 COAWST modeling system to couple different model components (Larson et al., 2004; Jacob et
112 al., 2005). A parallel-coupled approach is utilized by the coupler that permits the transmission and
113 transformation of various distributed parameters between component models. MCT coupler
114 facilitates exchanges of prognostic variables from one model to another model components.
115 Further details on various parameters exchanged among the component models of COAWST
116 modeling system can be found in Warner et al. (2010).

117 **2.2 Model configuration and experiment design**

118 The coupled model was configured over the BoB to study the VSCS Phailin during the
119 period of 10 to 15 October 2013. The setup of COAWST modeling system used in this study



120 included fully coupled atmosphere-ocean-wave (ROMS+WRF+SWAN) models but the sediment
121 transport is not included. A non-hydrostatic, fully compressible atmospheric model with a terrain
122 following vertical coordinate system, WRF-ARW (version 3.7.1) was used in COAWST
123 configuration. The atmospheric model used the parameterization schemes for calculating boundary
124 layer processes, precipitation processes, and surface radiation fluxes. The Monin-Obukhov scheme
125 of surface roughness layer parameterization (Monin and Obukhov 1954) was activated in the
126 model. The Rapid Radiation Transfer Model (RRTM) and cloud-interactive shortwave (SW)
127 radiation scheme from Dudhia (1989) were used. The planetary boundary layer scheme YSU-PBL,
128 described by Noh et al. (2003), was used. At each time step, the calculated value of exchange
129 coefficients and surface fluxes off the land or ocean surface by the atmospheric and land surface
130 layer models (NOAH) passed to the YSU PBL. The Grid-scale precipitation processes were
131 represented by WRF single-moment (WSM) six-class moisture microphysics scheme by Hong and
132 Lim (2006). The sub-grid scale convection and cloud detrainment were taken care by Kain (2004)
133 cumulus scheme.

134 A terrain following ocean model ROMS with 40 sigma levels used in this study. The
135 Generic-Length-Scale (GLS) vertical mixing scheme parameterized as the K- ϵ model used
136 (Warner et al., 2005). Tidal boundary conditions were derived from the TPXO.7.2
137 (<ftp://ftp.oce.orst.edu/dist/tides/Global>) data, which includes phase and amplitude of the M2, S2,
138 N2, K2, K1, O1, P1, MF, MM, M4, MS4, and MN4 tidal constituents along the east coast of India.
139 The tidal input was interpolated from TPXO.7.2 grid to ROMS computational grid. The
140 Shchepetkin boundary condition (Shchepetkin, 2005) for the barotropic current was used at open
141 lateral boundaries of the domain which allowed the free propagation of astronomical tide and wind
142 generated currents. The domains of atmosphere and ocean models which were part of the
143 COAWST modeling system are shown in Figure 1. The domain for SWAN model was similar to
144 the domain of ROMS model. The atmospheric model WRF had 9 km horizontal grid resolution
145 over the domain 65 °E-105 °E, 1°N-34 °N with 30 sigma levels in vertical. WRF was initialized
146 with National Centre for Environmental Prediction (NCEP) Final Analysis (FNL) data (NCEP-
147 FNL, 2000) on 10th October 2013 at 00 GMT. Lateral boundary conditions in WRF provided at 6-
148 h interval from the FNL data. The ROMS model domain had zonal and meridional grid resolutions
149 of 6 km and 4 km, respectively. The northern lateral boundary in ROMS was closed and the model
150 observed open boundaries in rest of the sides. The oceanic initial and lateral open boundary



151 conditions were derived from the Estimating the Circulation and Climate of the Ocean, Phase II
152 (ECCO2) data. Ocean bathymetry was derived from 2-minute gridded global relief data
153 (ETOPO2). The coupled modeling system allows exchange of prognostic variable among the
154 atmosphere, ocean, and wave models. The Advanced Very High Resolution Radiometer (AVHRR)
155 data was used for the validation of model simulated SST.

156 2.3. Methodology

157 The baroclinic current component was calculated by subtracting the barotropic component
158 from the mean current with a resolution of 2 m in the vertical. The power spectrum analysis was
159 performed on the zonal and meridional baroclinic currents along the depth section of the selected
160 location by using periodogram method. The continuous wavelet transform using Morlet wavelet
161 method carried out to analyze the temporal variability of the baroclinic current at a particular level
162 of 14 m. The near inertial baroclinic velocities were filtered by the Butterworth 2nd order scheme
163 for the cutoff frequency range of 0.033 to 0.043. The filtered zonal (u_f) and meridional (v_f) inertial
164 baroclinic currents were used to calculate the inertial baroclinic kinetic energy (E_f) in $m^2 s^{-2}$ and
165 inertial shear (S_f) following Zhang et al. (2014) using equation (1).

$$166 \quad S_f = \left(\frac{\partial u_f}{\partial z}\right)^2 + \left(\frac{\partial v_f}{\partial z}\right)^2 \quad (1)$$

167 As the stratification is a measure of oceanic stability, the buoyancy frequency (N) was calculated
168 using equation (2)

$$169 \quad N^2 = -\frac{g}{\rho} \frac{\partial \rho}{\partial z} \quad (2)$$

170 Where ρ is density of sea water and g is acceleration due to gravity.

171 The analysis of generation of the inertial oscillations and their dissipation was performed
172 on the basis of turbulent dissipation rate (ϵ) and turbulent eddy diffusivity (k_ρ). These parameters
173 were calculated by using following formula (Mackinnon and Gregg, 2005; van der Lee and
174 Umlauf, 2011; Palmer et al., 2008; Osborn, 1980)

$$175 \quad \epsilon = \epsilon_0 \left(\frac{N}{N_0}\right) \left(\frac{S_f}{S_0}\right) \quad (3)$$

$$176 \quad k_\rho = 0.2 x \left(\frac{\epsilon}{N^2}\right) \quad (4)$$



177 Where S_{if} is low shear background velocity, Values of $N_0 = S_0 = 3$ cycle per hour and $\varepsilon_0 = 10^{-8}$
178 $W \text{ kg}^{-1}$.

179 **3. Results and Discussion**

180 **3.1. Details of VSCS Phailin**

181 Phailin, a very severe cyclonic storm (VSCS) was developed over the BoB in northern
182 Indian Ocean in October 2013. The landfall of Phailin occurred on 12 October 2013 around 15:30
183 GMT near Gopalpur district of Odisha state at the east coast of India. After the 1999 super cyclonic
184 event of the Odisha coast, Phailin was the second strongest cyclonic event that made landfall at
185 east coast of India (Kumar and Nair, 2015). The low pressure system developed in the north of the
186 Andaman Sea on 7th October 2013, which transformed into a depression on 8th October at 12 °N,
187 96 °E. This depression got converted to a cyclonic disturbance on 9th October and further
188 intensified while moved to east-central BoB and opted the maximum wind speed of 200 km h^{-1} at
189 03:00 GMT on 11th October. Finally, landfall occur at 17:00 GMT 12th October. More details on
190 the development and propagation of VSCS Phailin can be found in literature (IMD Report, 2013;
191 Mandal et al. 2015; Prakash and Pant, 2016).

192 **3.2 Validation of coupled model simulations**

193 The WRF model simulated track of Phailin was validated against the India Meteorological
194 Department (IMD) reported best-track of the cyclone. A comparison of model simulated track with
195 the IMD track is shown in Figure 2. WRF model in the coupled configuration does fairly good job
196 in simulating the track of Phailin. The positional track error was about 40 km when compared to
197 IMD track of Phailin. The ROMS model simulated SST was validated against the Advance Very
198 High Resolution Radiometer (AVHRR) satellite data on each day for the period of Phailin passage
199 over the BoB. Figure 3 shows that the coupled model simulations are capturing the SST features
200 as well as the magnitude of cooling associated with the storm. The maximum cooling of the sea
201 surface observed on 13th October in the northwestern BoB in both, model and observations.

202 **3.3. Cyclone induced mixing**

203 The coupled atmosphere-ocean-wave simulation is an ideal tool to understand air-sea
204 exchange of fluxes and their effects on oceanic water column. Surface wind sets up currents on



205 the surface as well as initiate mixing in the interior of upper ocean. In order to examine the strength
206 of mixing due to VSCS Phailin, the model simulated vertical temperature profile together with the
207 zonal and meridional components of wind at a location 18.75 °N, 86.66 °E are plotted in Figure 4.
208 Temperature of the upper surface water (25 m -30 m) decreased by 3.5°C from its maximum value
209 of 28 °C after the landfall of cyclone on 12th October (Figure 4a). In response to the strong cyclonic
210 winds, the depth of 23 °C isotherm (D23) deepening from 50 m to 90 m was observed. At the same
211 time, the mixed layer depth (MLD) deepens by about 15 m. The inertial mixing introduced by the
212 cyclone play central role in deepening of D23 and MLD on 12th October 2013. To examine the
213 role of cyclone induced mixing in modulating the thermohaline structure of upper ocean, we
214 carried out further analysis on the coupled model simulations as discussed in the following
215 sections.

216 3.3.1. Kinetic energy distribution

217 During the initial phase of VSCS Phailin, the zonal and meridional currents were primarily
218 westward and southward, respectively (Figure 4b, 4c). However, on and after 12th October when
219 cyclone attains peak intensity and crosses over the location, alternative temporal sequences of
220 westward/eastward movement in zonal current and southward/northward flow in meridional
221 current were noticed in current profiles (Figures 4b, 4c). Frequency of these reversals in zonal and
222 meridional currents are recognized as near-inertial frequency generated from the storm at this
223 location (18.75 °N, 86.66 °E). The direction and magnitude of currents represent a variability
224 within 16-24 hr that corresponds to the near-inertial time period for the selected location. Kinetic
225 energy (KE) of currents at various depths is a proxy of energy available in water column that
226 becomes conducive for turbulent and inertial mixing. Time series of KE associated with the
227 barotropic and depth averaged baroclinic components of current at the point location (18.75° N,
228 86.66° E) are illustrated in Figure 4d. The KE associated with the baroclinic component found to
229 be much higher than the barotropic component of current. The depth averaged baroclinic and
230 barotropic current components' KE also depict the impinging oscillatory behavior. The peak
231 magnitude of KE in baroclinic and barotropic currents found to be $1.2 \text{ m}^2 \text{ s}^{-2}$ and $0.3 \times 10^{-2} \text{ m}^2 \text{ s}^{-2}$,
232 respectively on 12th October at 08:00 GMT. The analysis suggests that energy available for mixing
233 process in the water column was mostly confined in the baroclinic currents at various depths.

234



235 3.3.2. Primary frequency and depth of mixing

236 The power spectrum analysis was performed on the time series profiles at selected point
237 location (18.75 °N, 86.66 °E) to get distribution of all frequencies operating in the mixing process
238 during the passage of cyclone. As found in the previous section, the KE associated with baroclinic
239 currents are dominated over the barotropic currents, the power spectrum analysis performed on
240 zonal and meridional components of baroclinic current profile is shown in Figure 5. It is clear from
241 Figure 5 that tidal and near-inertial oscillations are two dominant frequencies on the surface during
242 the cyclone Phailin. Further, the near-inertial frequency is smaller than the tidal frequency on the
243 surface. To analyze the mixing potential of the NIO, power spectrum method was applied at the
244 profile of baroclinic current component (Figure 5). The largest power of the NIO was noticed at
245 14 m depth but the tidal oscillations were absent along the whole vertical section of baroclinic
246 current. This finding motivated to analyze the significance and distribution of these sub-surface
247 variability that resulted into anomalous deepening of MLD. Highest power of this signal was
248 associated within 0-15 m with magnitude of $0.84 \text{ m}^2 \text{ s}^{-1}$ in zonal baroclinic current and within 0-
249 38 m with magnitude of $0.76 \text{ m}^2 \text{ s}^{-1}$. These signals, however, weaken with increasing depth and
250 almost disappeared around 120 m depth. These NIO are the strongest signals at the 14 m depth
251 and dominating the mixing by any other process than the local wind stress.

252 In order to analyze the time distribution of the strong NIO, wavelet transform analysis was
253 applied on the zonal and meridional baroclinic currents at 14 m depth. The Scalogram, shown in
254 Figure 6, depicts the generation of NIO signal on 12th October that subsequently got strengthen
255 and attains its peak value on the mid of 13th October. The energy percentage of meridional
256 component was always lower than the zonal component. The peak values found in the time periods
257 between 25-28 hr marked with a white dashed line in Figure 6. A Butterworth 2nd order band pass
258 filter was applied at the corresponding cutoff frequency interval of 0.033 - 0.043 to filter the NIO
259 signal of the baroclinic zonal and meridional current. Figure 7 shows profiles of near-inertial zonal
260 (U_f) and meridional (V_f) baroclinic current together with the kinetic energy (E_f) of near-inertial
261 flow. The maximum strength of inertial baroclinic current was 0.3 m s^{-1} with the signature of an
262 alternate directional reversal of current signals. Presence of these inertial currents were up to 70 m
263 depth with peak value of kinetic energy E_f being $0.048 \text{ m}^2 \text{ s}^{-2}$. It can be noticed from Figure 7c,
264 the baroclinic kinetic energy remains higher ($> 0.03 \text{ m}^2 \text{ s}^{-2}$) only from mid of 11th October till the



265 end of 12th October and thereafter the energy rapidly decreases and almost disappeared after 13th
266 October. This indicates the period of prominent mixing due to NIO was 11-12 October 2013. The
267 daily averaged values of baroclinic kinetic energy (not shown here) also confirms the maxima in
268 E_f on 11-12 October with the vertical extent up to 80 m depth.

269 **3.3.3. Role of downward propagation of energy**

270 To investigate the energy propagation from surface to the interior layers of upper-ocean,
271 we derived the rotary spectra of near-inertial wave numbers and shown in Figure 8. The daily
272 averaged vertical wave-number rotary spectra provides a clear picture of wind energy distribution
273 in the sub-surface water. The anticyclonic spectrum is dominating over the cyclonic spectra for
274 entire duration of cyclone. This feature indicates that the energy is propagating downward
275 generated by these inertial oscillations. Magnitude of these oscillations increased from initial stage
276 up to 12th October and remained at high energy density for the rest of the cyclone period. This
277 downward directed energy initiated a process of mixing between the mixed layer and the
278 thermocline. This energy helps to deepen the mixed layer against oceanic stratification by
279 introducing a strong shear. The buoyancy of stratified ocean was overcome to some extent by the
280 shear generated that assist in mixing process during the very severe cyclone. For the current case,
281 kinetic energy (Figure 7c) represents the analogical behavior as reported by Alford and Gregg
282 (2001). Their study highlighted that, in most of the cases, the energy of inertial oscillations
283 potentially penetrates the mixed layer but suddenly drops down as it touches the thermocline. The
284 energy dissipation mechanism studied in few other studies (Chant, 2001; Jacob, 2003).

285 The 2-layer model described by Burchard and Rippeth (2009) illustrated the process of
286 generation of sufficient shear to start mixing near the thermocline. Their simple model ignored the
287 effect of lateral density gradient, mixing, and advection. Burchard et al. (2009) mentioned four
288 important parameters for shear generation, i.e. surface wind stress ($P_s S^2$), bed stress ($-D_b S^2$),
289 interfacial stress ($-D_i S^2$), barotropic flow ($P_m S^2$). Utilizing simulations from our coupled
290 atmosphere-ocean-wave model, we calculated individual terms as suggested by Burchard et al.
291 (2009) and presented in Figure 9. It is clear from the figure that the surface wind stress term plays
292 most significant role in modulating the magnitude of bulk shear during the stormy event. Other
293 terms were found to be relatively weaker and, therefore, contributing only marginally in the
294 variability of the bulk shear.



295 To examine the generation and dissipation of these inertial waves, the shear generated by
296 the near-inertial baroclinic current (S_f^2) and turbulent kinetic energy dissipation rate (ϵ) were
297 calculated and analyzed. The shear produced by inertial oscillations was increasing from 40-80 m
298 depth and higher magnitude was associated with peak wind speed of cyclone (Figure 10a). This
299 shear overcome the stratification (Figure 10b) that was weak at this depth compared to the shear
300 of the near-inertial waves. The value of ϵ increased from 4×10^{-14} to 2.5×10^{-13} W kg⁻¹ on
301 approaching the thermocline (Figure 10c). The increase in ϵ indicates weakening of the shear
302 generated by the inertial waves leading to fast disappearance of these baroclinic instabilities from
303 the region. The magnitude of the turbulent eddy diffusivity (K_ρ), shown in Figure 10d, implies that
304 the greater mixing takes place within the mixed layer place where K_ρ was high (6.3×10^{-11} to 1.2
305 $\times 10^{-11}$ m² s⁻¹). The daily averaged values of ϵ and K_ρ were 1.2×10^{-13} W kg⁻¹ and 1.5×10^{-10} m² s⁻¹,
306 respectively on 12th October, which were higher as compared to the initial two days of the cyclonic
307 event. Therefore, results from the present study as well as the conclusions from the past studies
308 indicate that wave-current interaction, mesoscale processes, and wave-wave interaction can affect
309 the process of downward mixing and cause the dissipation of inertial oscillations.

310 4. Conclusions

311 Processes controlling the sub-surface mixing were evaluated under the high wind speed
312 regime of a severe cyclonic storm Phailin over the BoB. A coupled atmosphere-ocean-wave
313 (WRF+ROMS+SWAN) model as part of the COAWST modeling system was used to simulate
314 atmospheric and oceanic conditions during the passage of Phailin cyclone. A detail analysis of
315 model simulated data revealed interesting features of generation, propagation, and dissipation of
316 kinetic energy in the upper oceanic water column. Deepening of the MLD and thermocline by 15
317 m and 40 m, respectively were explained through the strong shear generated by the inertial
318 oscillations that help to overcome the stratification and initiate mixing at the base of mixed layer.
319 However, there was a rapid dissipation of the shear with increasing depth below the thermocline.
320 Kinetic energy associated with baroclinic currents were about two order of magnitudes higher than
321 in barotropic component. The peak strength of 0.84 m² s⁻¹ in zonal baroclinic current was found at
322 14 m depth at a location in northwestern BoB. The wave-current interaction, mesoscale processes,
323 and wave-wave interaction were found to affect the process of downward mixing and cause the



324 dissipation of inertial oscillations. The coupled model found to be a useful tool to investigate air-
325 sea interaction and oceanic sub-surface processes.

326

327 **Author contribution:** KRP and TN performed model simulations and analyzed data. VP prepared
328 the manuscript with contributions from all co-authors.

329 **Acknowledgements**

330 ECCO2 is a contribution to the NASA Modeling, Analysis, and Prediction (MAP)
331 program. The study benefitted from the funding support from Ministry of Earth Sciences, Govt. of
332 India and Space Applications Centre, Indian Space Research Organisation. High Performance
333 Computing (HPC) facility provided by IIT Delhi and Department of Science and Technology
334 (DST), Govt. of India are thankfully acknowledged. Authors are thankful to Dr. Lingling Xie for
335 his productive suggestions. Graphics generated in this manuscript using Ferret and NCL. TN and
336 KRP acknowledge MoES and UGC-CSIR, respectively for their doctoral fellowship support.

337

338

339

340

341

342

343

344

345

346

347

348



349 **References**

- 350 Alam, M. M., Hossain, M.A. and Shafee, S.: Frequency of Bay of Bengal cyclonic storms and
351 depressions crossing different coastal zones, *Int. J. Climatol.*, 23, 1119–1125,
352 doi:10.1002/joc.927, 2003.
- 353 Alford, M.H., Gregg, M.C.: Near-inertial mixing: modulation of shear, strain and microstructure
354 at low latitude. *J. Geophys. Res.* 106 (C8), 16947–16968, 2001.
- 355 Booij, N., Ris, R. C., and Holthuijsen, L. H.: A third-generation wave model for coastal regions,
356 Part I, Model description and validation, *J. Geophys. Res.*, 104(C4), 7649–7666,
357 doi:10.1029/98JC02622, 1999.
- 358 Burchard, H., Rippeth, T.P.: Generation of bulk shear spikes in shallow stratified tidal seas. *J.*
359 *Phys. Oceanogr.* 39, 969–985, 2009.
- 360 Chang, J., Chung, C.-C., Gong, G.-C.: Influences of cyclones on chlorophyll-a concentration and
361 *Synechococcus* abundance in a subtropical western Pacific coastal ecosystem. *Mar. Ecol. Prog.*
362 *Ser.* 140, 199–205, 2008.
- 363 Chang, S. W., and Anthes, F.A.: The mutual response of the tropical cyclone and the ocean. *J.*
364 *Phys. Oceanogr.*, 9, 128–135, 1979.
- 365 Chant, R.J.: Evolution of near-inertial waves during an upwelling event on the New Jersey Inner
366 Shelf. *J. Phys. Oceanogr.* 31, 746–764, 2001.
- 367 Chassignet, E.P., Arango, H.G., Dietrich, D., Ezer, T., Ghil, M., Haidvogel, D.B., Ma, C.C.,
368 Mehra, A., Paiva, A.M., Sirkes, Z.: DAMEE-NAB: the base experiments. *Dyn. Atmos. Oceans*
369 32, 155–183, 2000.
- 370 Cione, J. J., and Uhlhorn, E.W.: Sea surface temperature variability in hurricanes: Implications
371 with respect to intensity change, *Mon. Weather Rev.*, 131, 1783–1796, doi:10.1175//2562.1,
372 2003.
- 373 Dudhia, J.: Numerical study of convection observed during the winter monsoon experiment using
374 a mesoscale two dimensional model. *J Atmos Sci* 46, 3077–3107, 1989.



- 375 Gill, A. E.: On the behavior of internal waves in the wake of storms, *J. Phys. Oceanogr.*, 14, 1129
376 – 1151, 1984.
- 377 Gonella, J.: A study of inertial oscillations in the upper layers of the oceans. *Deep-Sea Res.*, 18,
378 775–788, 1971.
- 379 Haidvogel, D.B., Arango, H.G., Budgell, W.P., Cornuelle, B.D., Curchitser, E., Di Lorenzo, E.,
380 Fennel, K., Geyer, W.R., Hermann, A.J., Lanerolle, L., Levin, J., McWilliams, J.C., Miller,
381 A.J., Moore, A.M., Powell, T.M., Shchepetkin, A.F., Sherwood, C.R., Signell, R.P., Warner,
382 J.C., Wilkin, J.: Regional ocean forecasting in terrain-following coordinates: model formulation
383 and skill assessment. *Journal of Computational Physics* 227, 3595–3624, 2008.
- 384 Haidvogel, D.B., Arango, H.G., Hedstrom, K., Beckmann, A., Malanotte-Rizzoli, P.
385 Shchepetkin, A.F.: Model evaluation experiments in the North Atlantic Basin: Simulations in
386 nonlinear terrain-following coordinates. *Dyn Atmos Oceans* 32, 239–281, 2000.
- 387 Hong, S.Y., Lim, J.O.J.: The WRF single-moment 6-class microphysics scheme (WSM6). *J*
388 *Korean Meteor Soc* 42:2, 129-151, 2006
- 389 IMD Report.: Very Severe Cyclonic Storm, PHAILIN over the Bay of Bengal (08-14 October
390 2013) A Report. India Meteorological Department, Technical Report, October 2013.
- 391 Jacob, S.D., Shay, L.K.: The role of oceanic mesoscale features on the tropical cyclone-induced
392 mixed layer response: A case study. *J. Phys. Oceanog.*, 33, 649- 676, 2003.
- 393 Jacob, R., Larson, J., Ong, E.: M x N Communication and Parallel Interpolation in CCSM Using
394 the Model Coupling Toolkit. Preprint ANL/MCSP1225-0205. Mathematics and Computer
395 Science Division, Argonne National Laboratory, 25 pp, 2005.
- 396 Johnston, T.M.S., Chaudhuri, D., Mathur, M., Rudnick, D.L., Sengupta, D., Simmons, H.L.,
397 Tandon, A., and Venkatesan, R.: Decay mechanisms of near-inertial mixed layer oscillations in
398 the Bay of Bengal, *Oceanography*, 29(2): 180–191, doi:10.5670/oceanog.2016.50, 2016.
- 399 Kirby, J. T., and Chen T.M.: Surface waves on vertically sheared flows: Approximate
400 dispersion relations, *J. Geophys. Res.*, 94(C1),1013–1027, doi:10.1029/JC094iC01p01013,
401 1989.



- 402 Kain, J.S.: The Kain-Fritsch convective parameterization: An update. *J Appl Meteor* 43, 170–
403 181, 2004.
- 404 Kumar VS, Nair A.M.: Inter-annual variations in wave spectral characteristics at a location off the
405 central west coast of India. *Ann Geophys* 33:159–167, doi:10.5194/angeo-33-159, 2015.
- 406 Latha, T.P., Rao, K.H., Nagamani, P.V., Amminedu, E., Choudhury, S.B., Dutt, C.B.S., and
407 Dadhwal, V.K.: Impact of Cyclone PHAILIN on chlorophyll-a concentration and productivity
408 in the Bay of Bengal. *International Journal of Geosciences* 6:473–480,
409 doi:10.4236/ijg.2015.65037, 2015.
- 410 Leipper, D. F.: Observed Ocean Conditions and Hurricane Hilda, 1964, *J. Atmos. Sci.*, 24, 182–
411 186, doi:10.1175/1520-0469(1967)0242.0.CO;2, 1967.
- 412 Zhi, Li., Yu, W., Li, T., Murty, V.S.N., and Tangang, F.: Bimodal character of cyclone
413 climatology in the Bay of Bengal modulated by monsoon seasonal cycle. *J Climate* 26:1033–
414 1046. doi: 10.1175/JCLI-D-11-00627.1, 2013.
- 415 Lin, I.I., Liu, W.T., Wu, C.C., Wong, T.F., Hu, C., Chen, Z., Liang, W.D., Yang, Y., Liu, K.K.:
416 New evidence for enhanced ocean primary production triggered by tropical cyclone. *Geophys.*
417 *Res. Lett.* 30 (13), doi:10.1029/2003GL017141, 2003.
- 418 Lin, I.I., Wu, C.C., Pun, I.F., Ko, D.S.: Upper ocean thermal structure and the western North
419 Pacific category-5 typhoons. Part I: ocean features and category-5 typhoon's intensification.
420 *Mon. Weather Rev.* 136, 3288–3306, 2008.
- 421 Longshore, D.: *Encyclopedia of Hurricanes, Typhoons, and Cyclones*, 468 pp., Checkmark, New
422 York, 2008.
- 423 Larson, J., Jacob, R., Ong, E.: The Model Coupling Toolkit: A New Fortran90 Toolkit for
424 Building Multiphysics Parallel Coupled Models. Preprint ANL/MCS- P1208-1204.
425 Mathematics and Computer Science Division, Argonne National Laboratory, 25 pp, 2004.
- 426 Lukas, R., and Lindstrom, E.: The mixed layer of the western equatorial Pacific Ocean, *J. Geophys.*
427 *Res.*, 96, 3343–3357, 1991.



- 428 MacKinnon, J.A., Gregg, M.C.: Mixing on the late-summer New England Shelf—solibores, shear
429 and stratification. *J. Phys. Oceanogr.* 33 (7), 1476–1492, 2003.
- 430 Mandal M., Singh K. S., Balaji M., Mohapatra M.: Performance of WRF-ARW model in real-
431 time prediction of Bay of Bengal cyclone ‘Phailin’. *Pure Appl. Geophys* DOI 10.1007/s00024-
432 015-1206-7, 2015.
- 433 Monin, A.S., Obukhov, A.M.F.: Basic laws of turbulent mixing in the surface layer of the
434 atmosphere. *Contrib Geophys Inst Acad Sci USSR* 151:163, e187, 1954.
- 435 National Centers for Environmental Prediction/National Weather Service/NOAA/U.S.
436 Department of Commerce: NCEP FNL Operational Model Global Tropospheric Analyses,
437 continuing from July 1999. Research Data Archive at the National Center for Atmospheric
438 Research, Computational and Information Systems Laboratory. Dataset.
439 <https://doi.org/10.5065/D6M043C6>, 2000.
- 440 Neetu, S., Lengaigne, M., Vincent, E.M., Vialard, J., Madec, G., Samson, G., Ramesh Kumar,
441 M.R., and Durand, F.: Influence of upper-ocean stratification on tropical cyclone-induced
442 surface cooling in the Bay of Bengal, *J. Geophys. Res.*, 117, C12020,
443 doi:10.1029/2012JC008433, 2012.
- 444 Noh, Y., Cheon, W.G., Hong, S.Y., Raasch, S.: Improvement of the K-profile model for the
445 planetary boundary layer based on large eddy simulation data. *Bound Layer Meteor* 107, 401–
446 427, 2003.
- 447 Osborn, T.R.: Estimates of the Local-Rate of Vertical Diffusion from Dissipation Measurements.
448 *J. Phys. Oceanogr.* 10, 83–89, 1980.
- 449 Palmer, M.R., Rippeth, T.P., Simpson, J. H.: An investigation of internal mixing in a seasonally
450 stratified shelf sea. *J. Geophys. Res.* 113, C12005, doi:10.1029/2007JC004531, 2008.
- 451 Pant V, Girishkumar M.S., Udaya Bhaskar T.V.S., Ravichandran M., Papa F., Thangaprakash
452 V.P.: Observed interannual variability of near-surface salinity in the Bay of Bengal, *J. Geophys.*
453 *Res* 120(5):3315–3329, 2015.



- 454 Prakash K.R., Vimlesh Pant: Upper oceanic response to tropical cyclone Phailin in the Bay of
455 Bengal using a coupled atmosphere-ocean model, *Ocean Dynamics*, 67, 51-64,
456 doi:10.1007/s10236-016-1020-5, 2017.
- 457 Price, J. F., Mooers, C.N., and Van Leer, J.C.: Observation and simulation of storm-induced
458 mixed-layer deepening. *J. Phys. Oceanogr.*, 8, 582-599, [https://doi.org/10.1175/1520-](https://doi.org/10.1175/1520-0485(1978)008<0582:OASOSI>2.0.CO;2)
459 [0485\(1978\)008<0582:OASOSI>2.0.CO;2](https://doi.org/10.1175/1520-0485(1978)008<0582:OASOSI>2.0.CO;2), 1978.
- 460 Price, J.F.: Upper ocean response to a hurricane. *J. Phys. Oceanogr.*, 11, 153-175, 1981.
- 461 Rao, R. R., and Sivakumar, R.: Seasonal variability of sea surface salinity and salt budget of the
462 mixed layer of the north Indian Ocean, *J. Geophys. Res.*, 108(C1), 3009,
463 doi:10.1029/2001JC000907, 2003.
- 464 Sanford, T. B., Black, P.G., Haustein, J., Feeney, J.W., Forristall, G.Z., and Price, J.F.: Ocean
465 response to a hurricane. Part I: Observations. *J. Phys. Oceanogr.*, 17, 2065–2083, 1987.
- 466 Sarangi, R. K.: Remote-sensing-based estimation of surface nitrate and its variability in the
467 southern peninsular Indian waters, *Int. J. Oceanogr.*, doi:10.1155/2011/172731, 2011.
- 468 Shang, S., Li, L., Sun, F., Wu, J., Hu, C., Chen, D., Ning, X., Qiu, Y., Zhang, C., and Shang, S.,
469 Changes of temperature and bio-optical properties in the South China Sea in response to
470 Typhoon Lingling, (2001), *Geophys. Res. Lett.*, 35, L10602, doi:10.1029/2008GL033502,
471 2008.
- 472 Shchepetkin and A. F., McWilliams J. C.: The Regional Ocean Modeling System: A split-explicit,
473 free-surface, topography following coordinates ocean model, *Ocean Modelling*, 9, 347-404,
474 2005.
- 475 Skamarock, W.C., Klemp, J.B., Dudhia, J., Gill, D.O., Barker, D.M., Wang, W., Powers, J.G.:
476 A Description of the Advanced Research WRF Version 2. NCAR Technical Note, NCAR/TN-
477 468+STR., 2005.
- 478 Shay, L. K., Black, P., Mariano, A., Hawkins, J., and Elsberry, R.: Upper ocean response to
479 hurricane Gilbert, *J. Geophys. Res.*, 97(20), 227–248, 1992.



- 480 Shay, L. K. and Elsberry, R.L.: Vertical structure of the ocean current response to a hurricane. J.
481 Phys. Oceanog., 19, 649-669, 1989.
- 482 Shay, L. K., Goni, G.J., and Black, P.G.: Effects of a warm oceanic feature on Hurricane Opal,
483 Mon. Weather Rev., 128, 1366–1383, doi:10.1175/1520-0493(2000)128<1366:CO>2.0.CO;2, 2000.
- 484 Shearman, R.K.: Observations of near-inertial current variability on the New England shelf. J.
485 Geophys. Res. 110, C02012, doi:10.1029/2004JC002341, 2005.
- 486 Suzana, J Carmargo, Adam H Sobel, Anthony G Barnston and Kerry A. Emanuel: Tropical
487 cyclone genesis potential index in climate models. Tellus 59A:428-443, 2007.
- 488 Thadathil, P., Muraleedharan, P.M., Rao, R.R., Somayajulu, Y.K., Reddy, G.V., and
489 Revichandran, C.: Observed seasonal variability of barrier layer in the Bay of Bengal, J.
490 Geophys. Res., 112, C02009, doi:10.1029/2006JC003651, 2007.
- 491 Varkey, M. J., Murty, V.S.N., and Suryanarayana, A.: Physical oceanography of the Bay of Bengal
492 and Andaman Sea, Oceanogr. Mar. Biol., 34, 1–70, 1996.
- 493 van der Lee, E.M., and Umlauf, L.: Internal wave mixing in the Baltic Sea: near-inertial waves in
494 the absence of tides. J. Geophys. Res. 116, C10016, doi:10.1029/2011JC007072, 2011.
- 495 Vinayachandran, P. N., Murty, V.S.N., and Ramesh Babu V.: Observations of barrier layer
496 formation in the Bay of Bengal during summer monsoon, J. Geophys. Res., 107(C12), 8018,
497 doi:10.1029/2001JC000831, 2002.
- 498 Vissa, N.K., Satyanarayana, A.N.V. and Prasad Kumar, B.: Intensity of tropical cyclones during
499 pre- and post-monsoon seasons in relation to accumulated tropical cyclone heat potential over
500 Bay of Bengal, Nat Hazards 68: 351. <https://doi.org/10.1007/s11069-013-0625-y>. 2013.
- 501 Warner, J. C., Sherwood, C.R., Arango, H.G., and Signell, R.P.: Performance of four turbulence
502 closure models implemented using a generic length scale method, Ocean Modell., 8, 81–113,
503 doi:10.1016/j. ocemod.2003.12.003, 2005.
- 504 Warner, J.C., Armstrong B., He R., Zambon J.B.: Development of a coupled ocean–
505 atmosphere–wave–sediment transport (COAWST) modeling system. Ocean modelling 35:230–
506 244. doi:10.1016/j. oceanmod.2010.07.010, 2010.



507 Yanase, W., Satosh, M., Taniguchi, H., and Fujinami, H.: Seasonal and Intraseasonal Modulation
508 of tropical cyclogenesis environment over the Bay of Bengal during the extended summer
509 monsoon. *J Climate* 25:2914-2930. doi: 10.1175/JCLI-D-11-00208.1, 2012.

510 Zhang, S., Xie, L., Hou, Y., Zhao, H., Qi, Y., & Yi, X.: Tropical storm-induced turbulent mixing
511 and chlorophyll-a enhancement in the continental shelf southeast of Hainan Island. *Journal of*
512 *Marine Systems*, 129, 405-414, 2014.

513 Zhao, H., Tang, D.L., Wang, D.X.: Phytoplankton blooms near the Pearl River Estuary induced
514 by Typhoon Nuri. *J. Geophys. Res.* 114, C12027, doi:10.1029/2009JC005384, 2009.

515

516

517

518

519

520

521

522

523

524

525

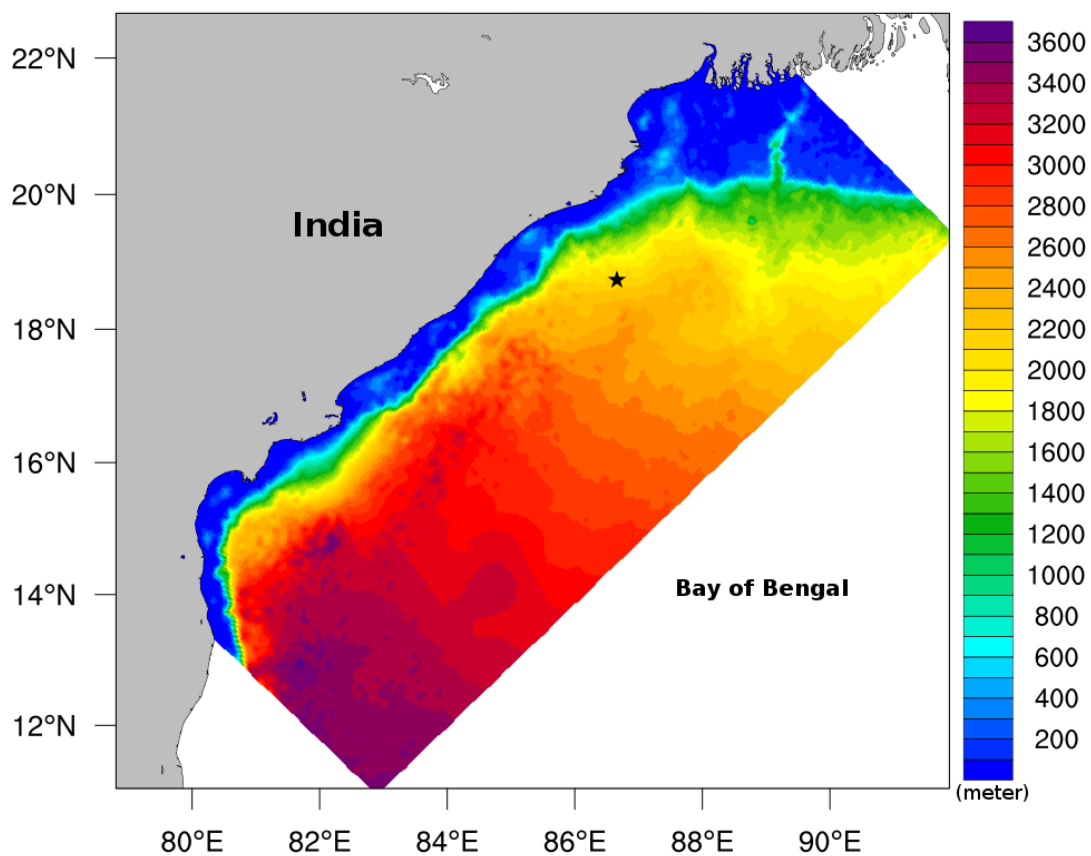
526

527

528

529

530



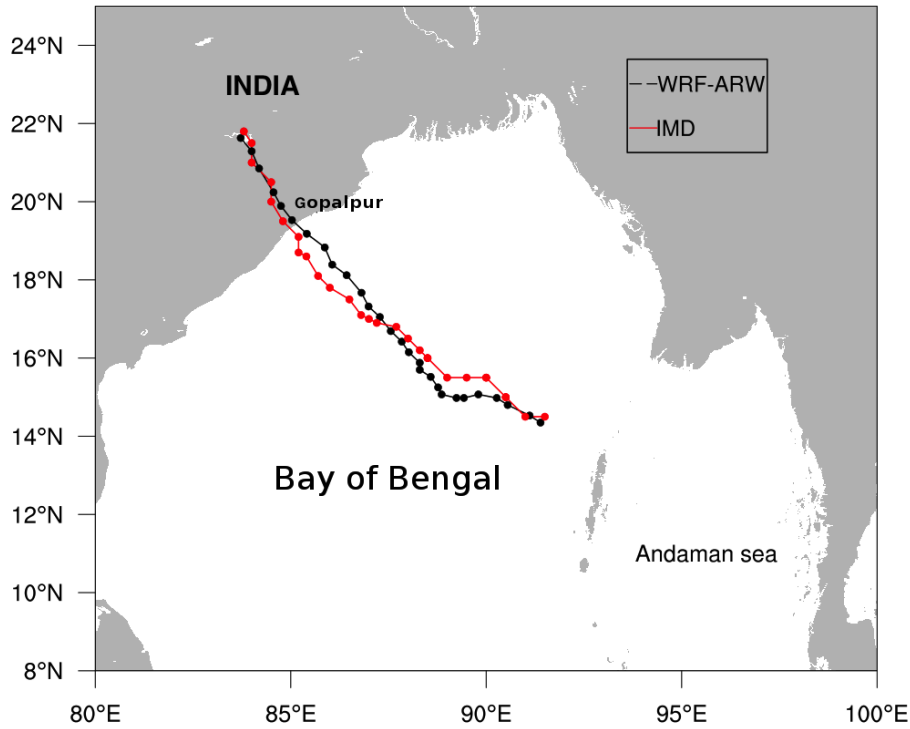
531

532 **Figure 1:-COAWST model domain (65°-105 °E, 1°-34 °N) overlaid with GEBCO bathymetry (m).**
533 **Location used for time-series analysis marked with a star.**

534

535

536

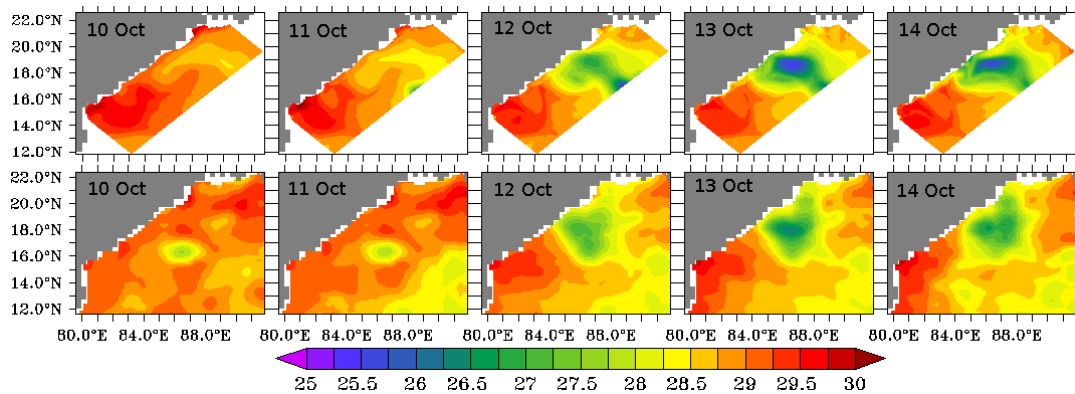


537

538 **Figure 2:- Validation of VSCS Phailin track simulated by coupled model (black) with IMD**
 539 **reported track (red).**

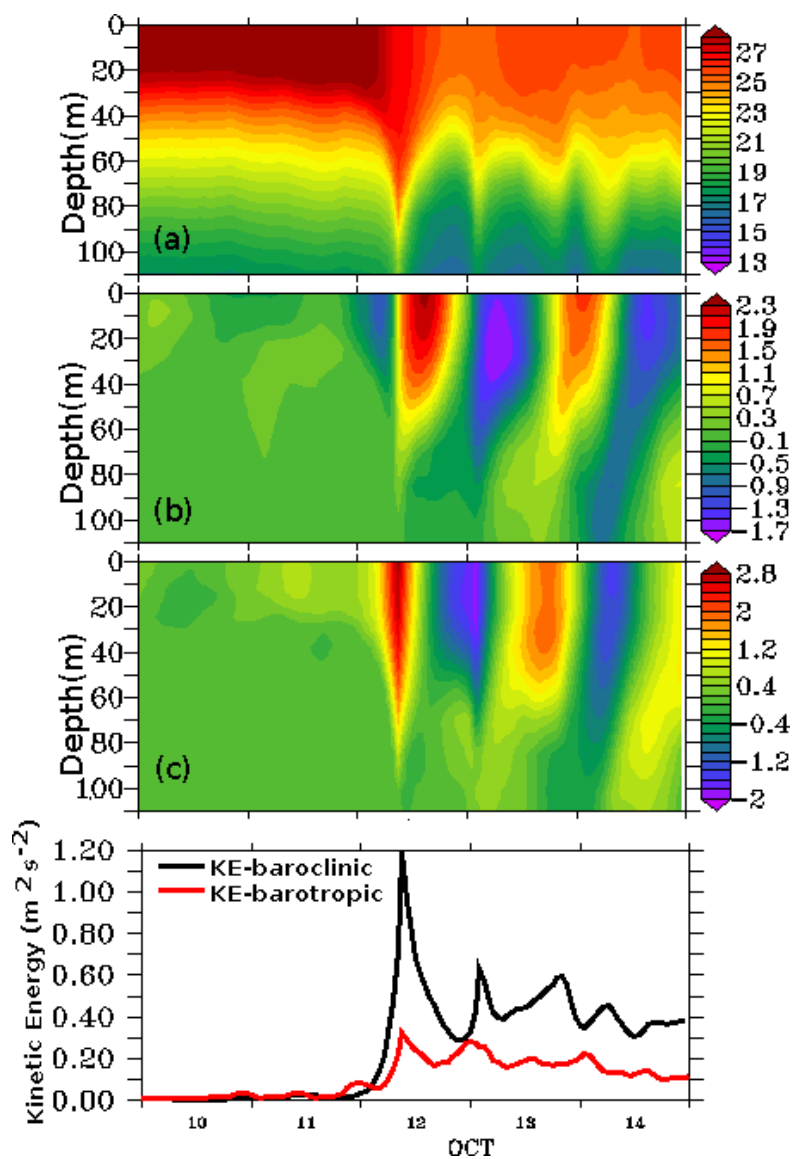
540

541



542

543 **Figure 3:- Sea Surface Temperature (SST) in °C observed from AVHRR satellite (lower panel) and**
 544 **simulated by model (upper panel).**



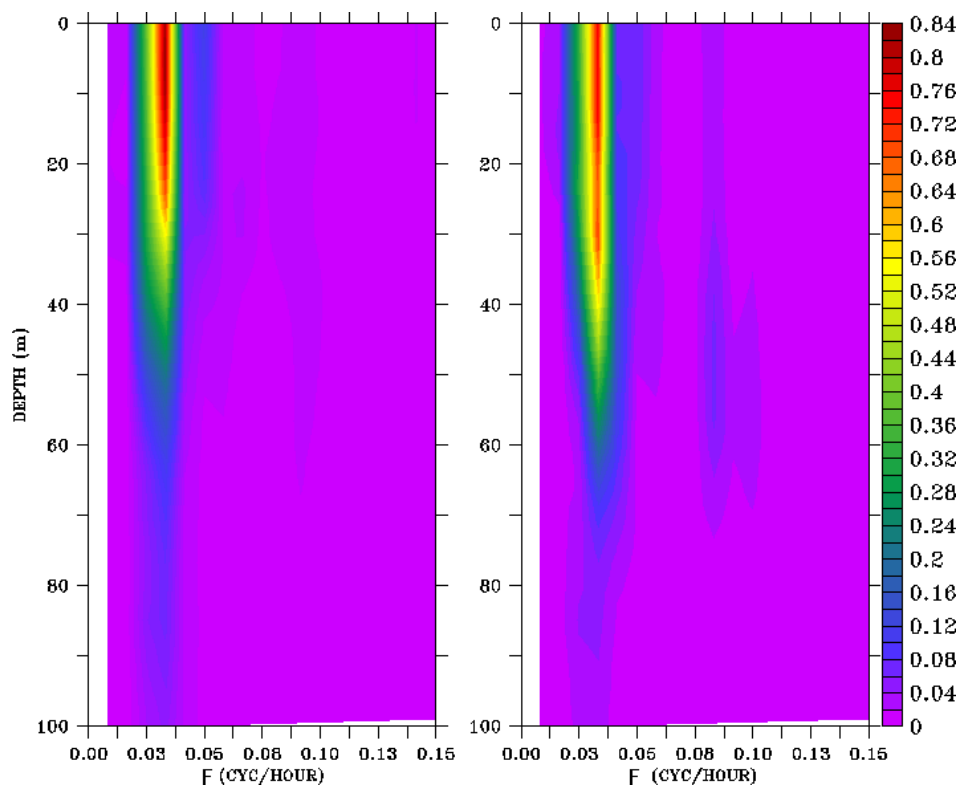
545

546 **Figure 4:- The vertical profiles of temperature in $^{\circ}\text{C}$ (a), zonal current in m s^{-1} (b), meridional**
547 **current in m s^{-1} (c). The kinetic energy (m^2s^{-2}) of baroclinic current (black) and barotropic current**
548 **($\times 10^{-2}$) (red).**

549

550

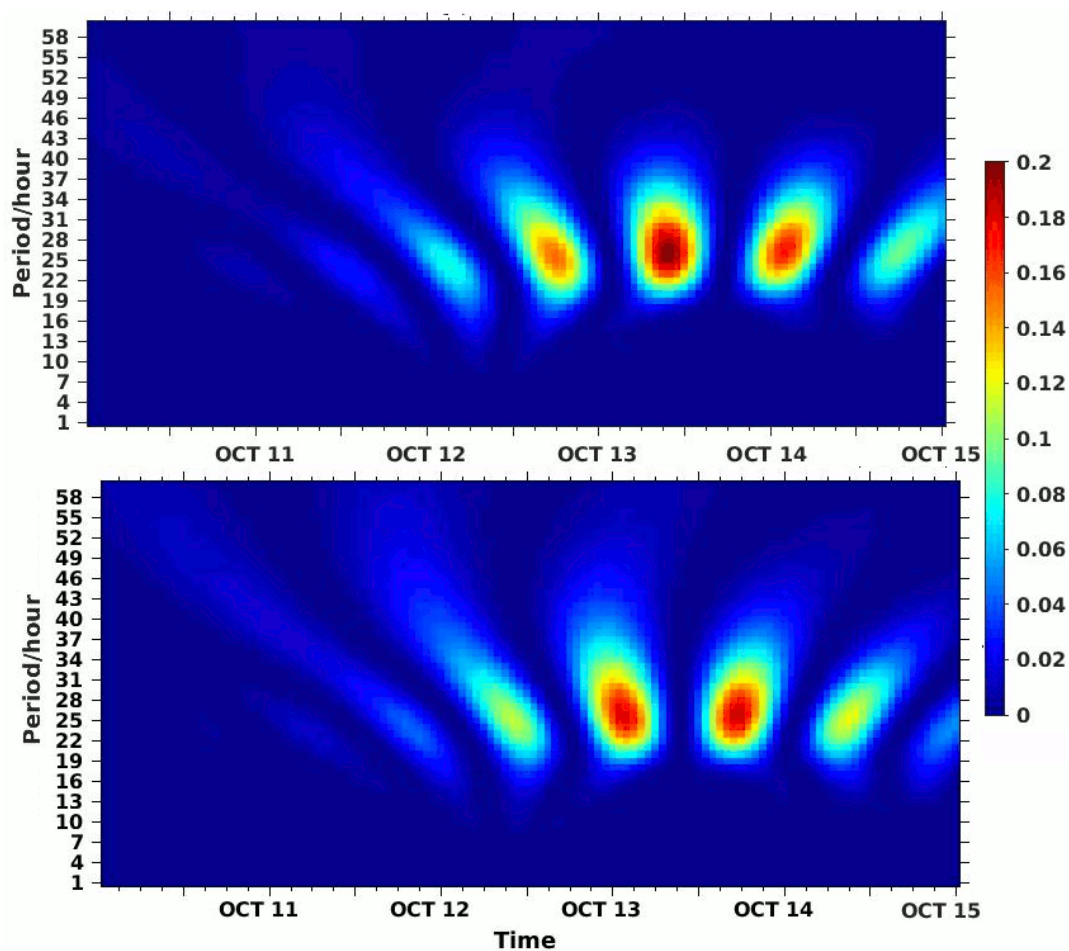
551



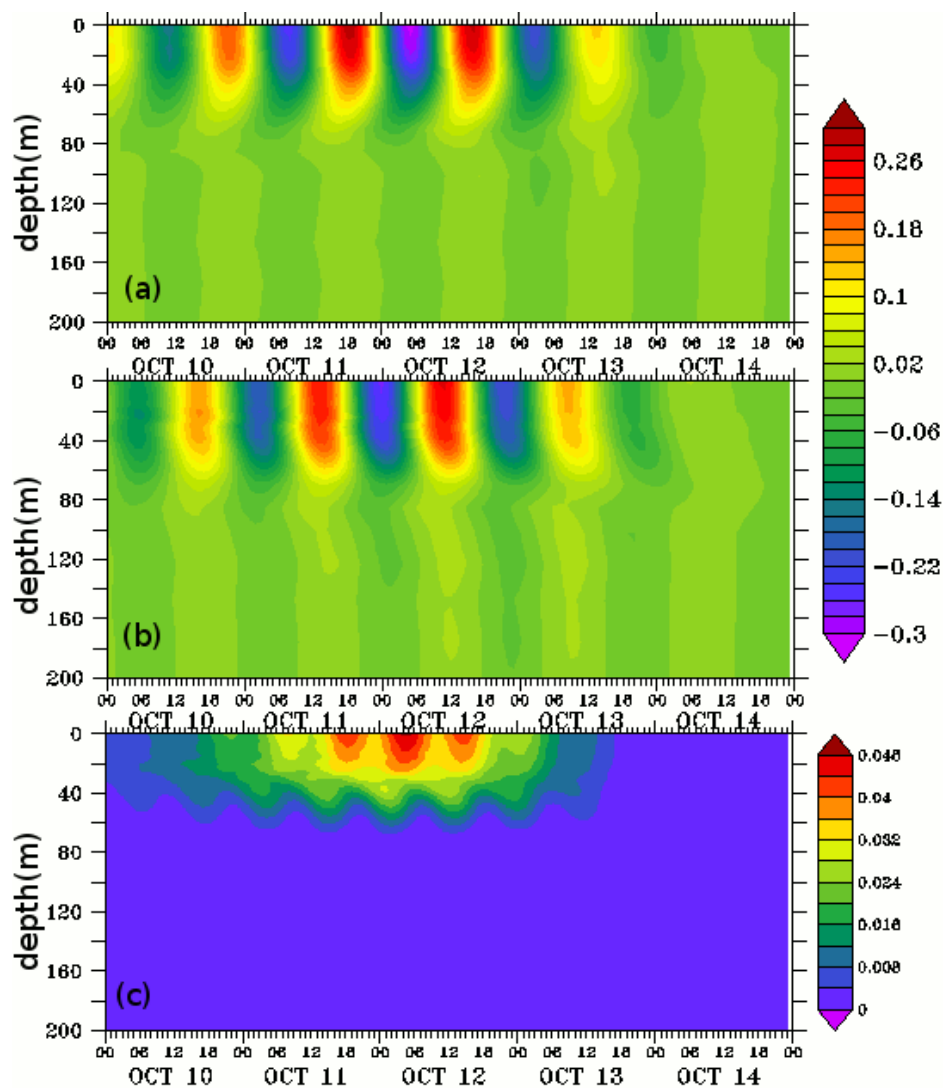
552

553 **Figure 5:- The power spectrum analysis (m^2s^{-1}) for a) baroclinic zonal current and b) baroclinic**
554 **meridional current**

555



556
557 **Figure 6:-** The scalogram in percentage at 40 m depth by continuous wavelet transform (CWT)
558 **method.** Wavelet scalogram shown for the zonal baroclinic current (upper panel) and for the
559 **meridional baroclinic current (lower panel).** The white dashed line indicates the peak percentage of
560 **energy.**



561

562 **Figure 7:-** The profiles of a) near inertial zonal baroclinic current (U_f) b) near inertial meridional
563 current (V_f) in $m\ s^{-1}$ and c) Kinetic energy (E_f) of near inertial flow in m^2s^{-2}

564

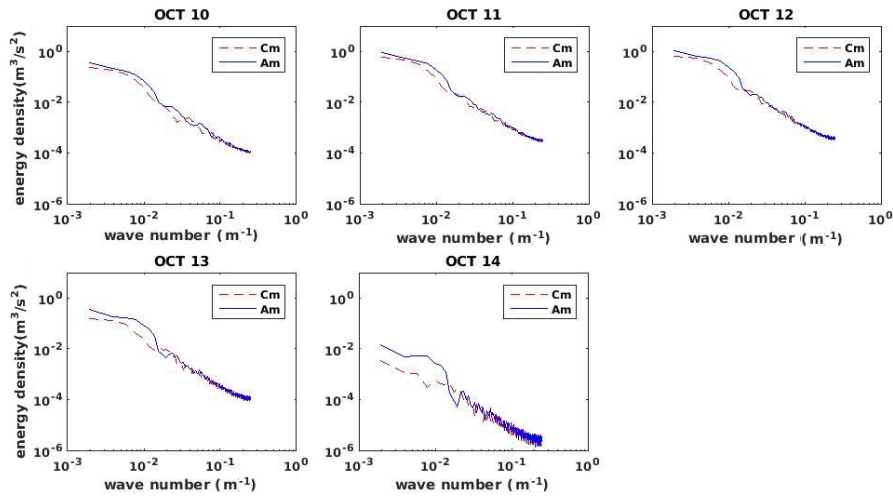
565

566

567

568

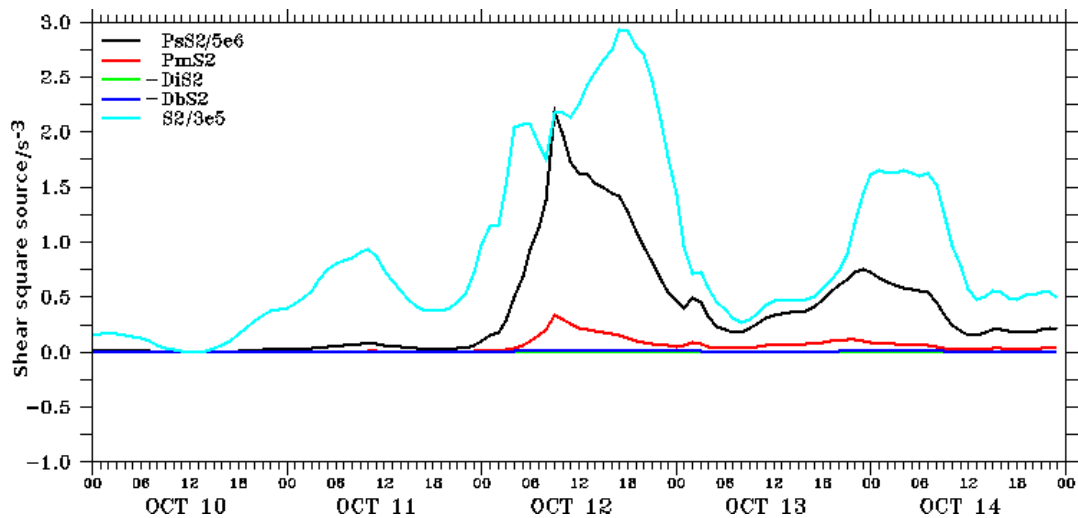
569



570

571 **Figure 8:- The daily averaged vertical wave-number rotary spectra of near inertial oscillations. The**
 572 **anticyclonic and cyclonic spectra are represented in blue and dotted red lines respectively.**

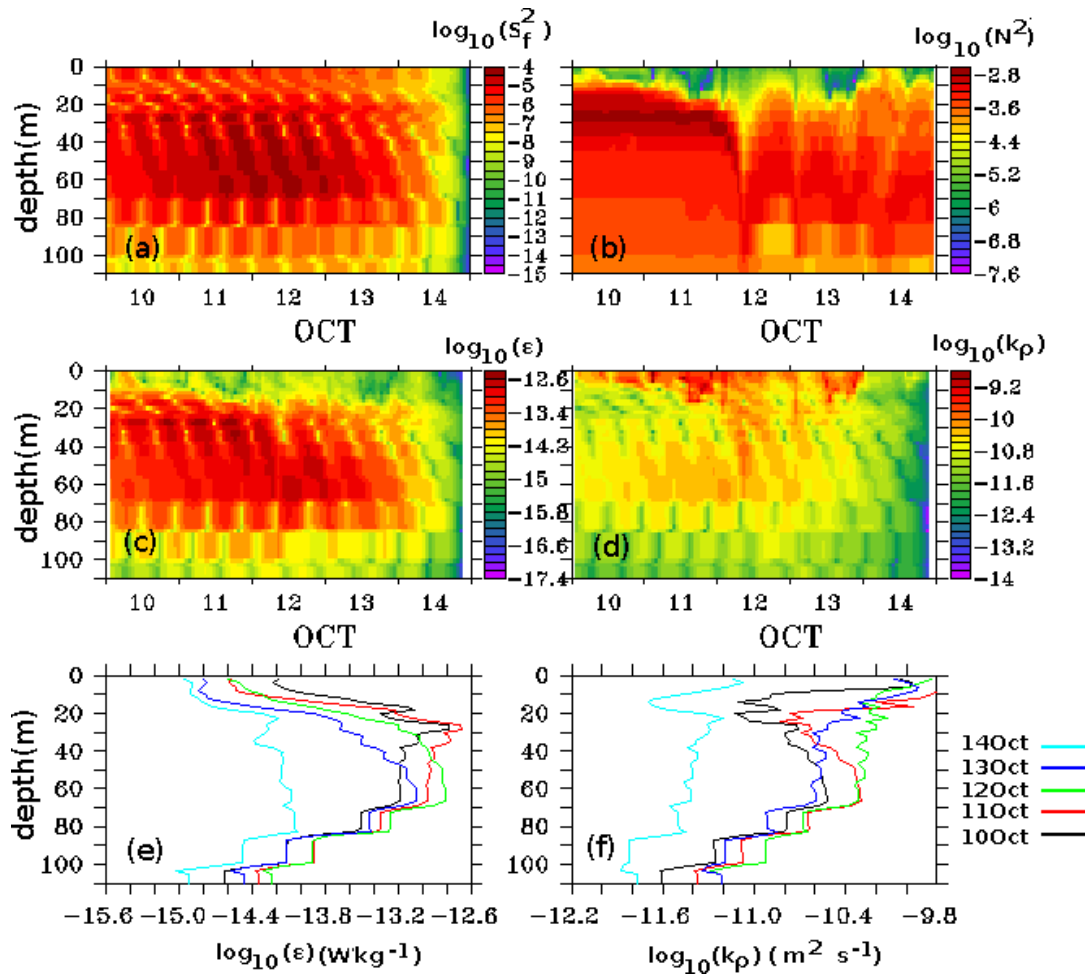
573



574

575 **Figure 9:- The model simulated bulk properties at the selected point location. The vertical shear**
 576 **square axis is multiplied with a factor of 10^{-6} . The magnitude of bulk shear squared S^2 (cyan color),**
 577 **surface wind stress $P_s S^2$ (black color), barotropic effect $P_m S^2$ (red color), bottom stress $-D_b S^2$ (blue**
 578 **color), interfacial friction $-D_i S^2$ (green color)**

579



580

581 **Figure 10:- Profiles of a) velocity shear $\log_{10}(S^2)$, b) buoyancy frequency $\log_{10}(N^2)$, c) turbulent kinetic**
 582 **energy dissipation rate $\log_{10}(\epsilon)$, d) turbulent eddy diffusivity $\log_{10}(K_p)$, e) and f) are daily averaged**
 583 **turbulent kinetic energy dissipation rate and turbulent eddy diffusivity respectively**

584